



Contents lists available at ScienceDirect

Gondwana Research

journal homepage: www.elsevier.com/locate/gr

On the allochthonous nature of auriferous greenstones, Guayana shield, Venezuela



Robert S. Hildebrand^{a,*}, Robert Buchwaldt^b, Samuel A. Bowring^b

^a Department of Geology, University of California, One Shields Ave., Davis, CA 95616-8605, USA

^b Department of Earth, Atmospheric, and Planetary Sciences, Massachusetts Institute of Technology, Cambridge, MA 02139, USA

ARTICLE INFO

Article history:

Received 2 July 2013

Received in revised form 16 September 2013

Accepted 17 September 2013

Available online 11 October 2013

Handling Editor: T. Kusky

Keywords:

Guayana shield

Tectonics

Greenstones

Gold

Allochthons

ABSTRACT

The tectonic style of Paleoproterozoic orogeny in the Guayana shield has been considered by most workers to be similar to those commonly invoked for the development of Archean greenstone belts, in which diapirs of granitoid magma (Supamo complex) rose and deformed 2.1–2.0 Ga volcanic and sedimentary rocks of the Pastora supergroup to form keel-like greenstone belts. In this model, subsequent collision with the dominantly granulite-grade Imataca complex to the north deformed the greenstone belts during what is known as the Trans-Amazonian orogeny. However, more recent geological mapping demonstrated that the base of the greenstone belts is marked by a major mylonitic shear zone that placed rocks of the belts atop a regional unit of quartzite that sits unconformably upon granitic gneisses and plutons of both the Imataca and Supamo complexes. These relations were interpreted to indicate that the greenstone belts are allochthonous with respect to the Imataca and Supamo complexes, and as the quartzite oversteps the contact between the Imataca and Supamo complexes, juxtaposition of the two complexes predated deposition of the quartzite. New U–Pb zircon results show that volcanic rocks of the Pastora supergroup are older than the quartzite beneath them and confirm the hypothesis, based entirely upon field relations, that rocks of the greenstone belts were thrust upon the quartzite and its granitic and gneissic basement. At least two subsequent periods of deformation refolded rocks of the region. Similar structural relationships are common in Archean cratons of southern Africa, Australia, and the Canadian shield.

© 2013 International Association for Gondwana Research. Published by Elsevier B.V. All rights reserved.

1. Introduction

Although legions of books and films romanticized the Californian and Klondike gold rushes, the most productive gold mine in the world during the latter part of the 19th century was the El Callao mine of Venezuela (Sidder, 1990). El Callao is located within the Guayana shield of northeastern South America, a region well known for hosting rich gold-bearing veins and shear zones (Orris et al., 1993; Haines, 2004). Although there are abundant small placer mines, the bulk of the mined gold occurred in ductile to brittle fault zones within Paleoproterozoic greenschist grade volcano-sedimentary belts referred to as greenstone belts. The greenstone belts comprise mostly mafic-intermediate composition pillowed and subaerial lava and are surrounded by a sea of granitic gneisses and plutons. In this regard they are similar to typical Archean greenstone–granite terranes common to shield regions worldwide.

The greenstone belts within the Guayana shield were considered by previous workers to have formed when rising masses of magma metamorphosed, deformed, and isolated the older volcano-sedimentary succession into discrete belts separated by domical plutons (Mendoza, 1977; Cox et al., 1993; Sidder and Mendoza, 1995; Mendoza, 2000). However, detailed mapping, combined with regional reconnaissance,

led to the recognition that a regional quartzite unit sits unconformably upon the granitic rocks and is separated from the overlying greenstone belts by a major ductile fault, which Hildebrand (2005) suggested formed when the volcano-sedimentary packages of the Pastora supergroup were thrust over the veneer of quartzite sitting atop the granitic gneisses and plutons of the Supamo terrane. These thrusts demonstrate large-magnitude horizontal movement of at least 100 km.

In the “traditional” model the granites and gneisses of the Supamo terrane must be younger than the volcanic and sedimentary rocks of the Pastora supergroup. In the Hildebrand (2005) model, there is no such requirement as rocks of the Supamo terrane and Pastora supergroup were juxtaposed structurally after formation.

During fieldwork we collected several samples suitable for U–Pb geochronology to prove or disprove the new tectonic model. Here we report the results of our U–Pb zircon dating and then briefly discuss their impact on gold exploration and regional tectonic models. Finally, we compare the resulting model to those of granite–greenstone belts worldwide.

2. Geology

The Guayana shield is located in northeastern South America, where it forms the northernmost part of the Amazonian shield (Fig. 1). Prior to the opening of the Atlantic ocean this cratonic block and the Birimian

* Corresponding author.

E-mail address: rsildebrand@ucdavis.edu (R.S. Hildebrand).

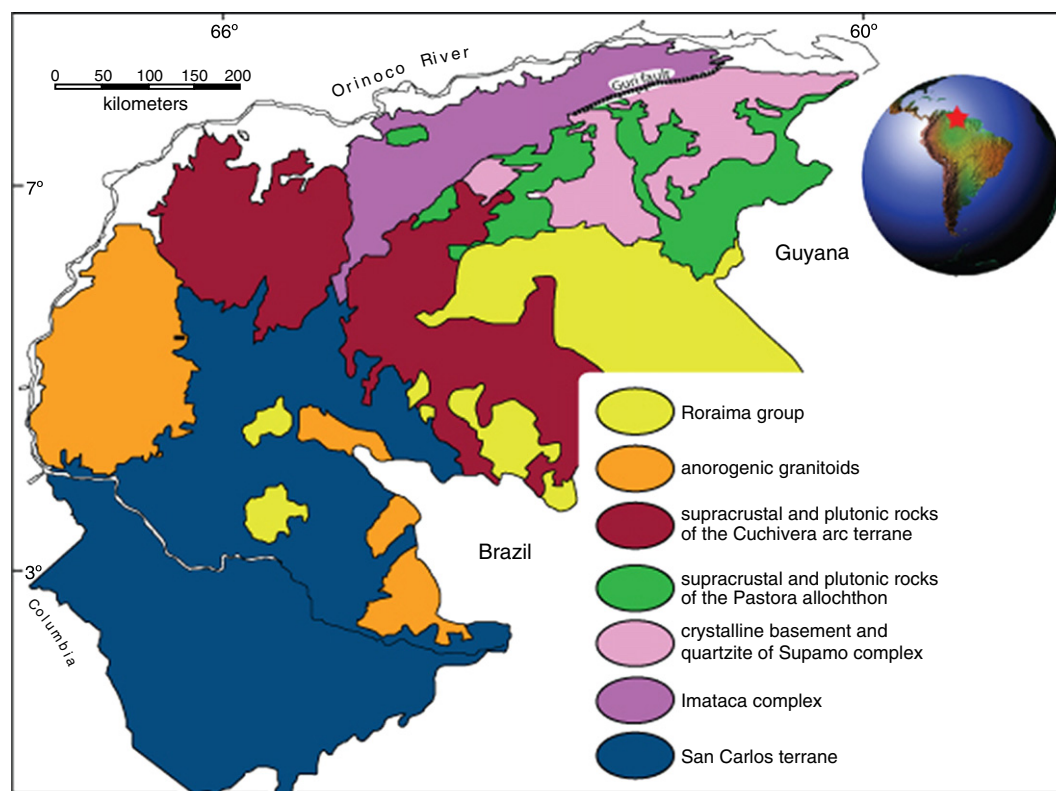


Fig. 1. Regional map illustrating the various terranes of the Guayana shield within southeastern Venezuela. This paper focuses on the Imataca and Supamo complexes and Pastora supergroup of the northeastern part of the shield.

system of West Africa formed an extensive Paleoproterozoic cratonic area within Pangea (Hurley et al., 1976; Smith and Livermore, 1991; Cordani and Teixeira, 2007).

The Guayana shield is perhaps best known for its tepuis, which are mesas composed of flat-lying 1.87 Ga sandstones of the Roraima Group (Santos et al., 2003) that rise up to 1 km above older basement rocks. The tepuis are remnants of a much larger region of Paleoproterozoic cover rocks and contain remarkable endemic species (Gleason and Killip, 1938); were the inspiration for *The Lost World* (Doyle, 1912); and host Angel Falls, the world's tallest waterfall (Robertson, 1949; Angel, 2012).

Lying unconformably beneath the sandstones are a wide variety (Fig. 1) of Archean and Paleoproterozoic rocks: (1) the Imataca complex, dominated by Archean granulite to amphibolite facies gneisses; (2) the Pastora–Supamo terrane, a Paleoproterozoic granite–greenstone terrane which is the main subject of this paper; (3) another Paleoproterozoic basement assemblage of granitoids, gneisses and minor volcanic rocks called the San Carlos terrane; and (4) a northwesterly-trending, Paleoproterozoic, calc-alkaline, volcano–plutonic complex, the Cuchivero, that sits unconformably upon both the San Carlos and Imataca–Pastora–Supamo terranes. Gabbroic and doleritic intrusions, known as the Avanavero suite, intruded rocks of the Roraima group and its basement at 1.79 Ga, and there is a Mesoproterozoic suite of anorogenic rapakivi granites.

The Imataca complex comprises mostly isoclinally folded migmatitic felsic granulite and quartzo-feldspathic orthogneiss at amphibolite grade with lesser amounts of paragneiss and mafic granulite (Dougan, 1977; Tassinari et al., 2004). The Supamo complex, or terrane, consists of migmatitic and gneissic granitic rocks, dominantly granodioritic to quartz dioritic with lesser quantities of paragneiss and schist. The Supamo complex is not known to host mineral deposits (Orris et al., 1993).

A regional quartzite unit (Figs. 2, 3a,b), that Hildebrand (2005) named the El Miamo Formation, was deposited upon eroded rocks of both the Imataca and Supamo terranes, which, if the quartzites are the

same unit on both terranes, indicates that they were juxtaposed prior to deposition of the quartzite. Although locally the quartzite has heavy minerals defining cross-stratification, the unit is extensive and pure enough that it is strip-mined for silica to be used in the iron smelters along the Orinoco River at Puerto Ordaz (Fig. 3c). Sitting atop the quartzite are 3–15 m of mafic amphibolite-grade ultramylonite (Fig. 3d, e) that passes progressively upwards into less penetratively strained greenschist grade mafic rocks (Fig. 3f) of the Pastora supergroup. Intermediate-mafic rocks of the Pastora supergroup form tree-covered hills whereas siliceous volcanics of the supergroup, as well as gneisses and granitoids of the Supamo complex, are dominantly flat plains covered by savanna-type vegetation due to breakdown of potassium feldspar during deep tropical weathering (Fig. 3g).

As originally defined, the Pastora supergroup comprises the Carichapa group and the overlying Yuruari formation (Menéndez, 1968). The Carichapa group consists of the El Callao and Cicapra formations. Thickness estimates for formations are unreliable due to high penetrative strain, faults and folds. Contacts between formations are dominantly structural, rarely stratigraphic. Thus, it is entirely possible that rocks of the Yuruari formation are the same age as, or older than, rocks of the El Callao formation.

The El Callao formation (Korol, 1965; Menéndez, 1968) occupies the structurally lowest thrust slices and is dominated by pillowed and massive tholeiitic basalt-basaltic andesite with associated pillow breccias and minor chert. The rocks were metamorphosed to greenschist facies assemblages of biotite–chlorite–albite–epidote–actinolite but within the mylonitic rocks of the basal thrust the rocks reach the amphibolite facies. The slabby nature of the amphibolite grade mylonites makes them a favorite facing stone for walls and flooring of most town plazas in the area so that many small artisanal quarries provide good exposures.

The Yuruari formation (Korol, 1965) is dominated by epiclastic and volcanic rocks metamorphosed and deformed to schists with greenschist facies assemblages of chlorite–sericite–calcite. Original lithologies were feldspathic sandstone, siltstone and shale with minor chert, tuff breccia

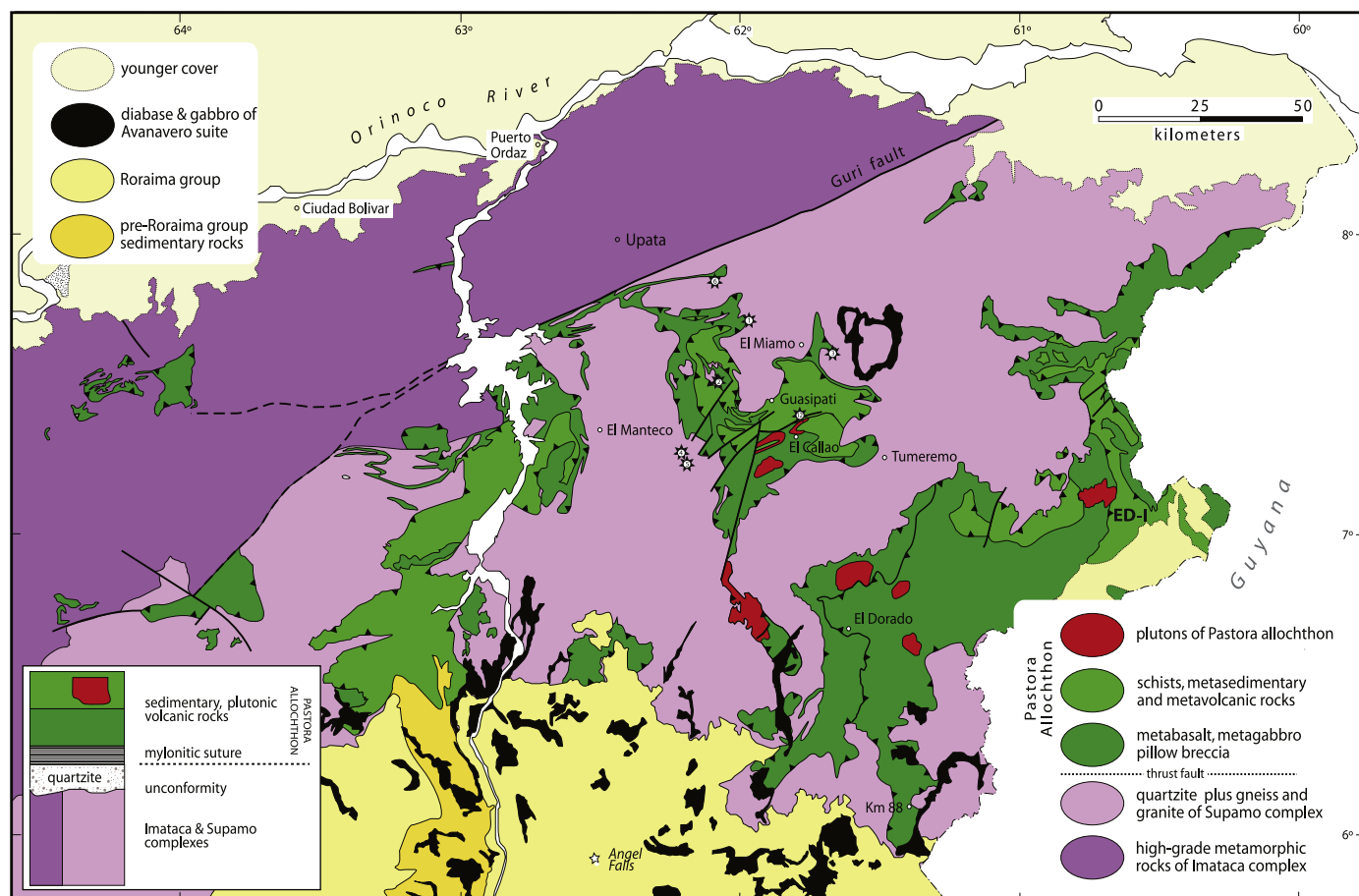


Fig. 2. A more detailed geological map showing the northeast corner of the Guayana shield in Venezuela and units discussed in the text. Lower left inset: a schematic column showing the relations based on mapping by Hildebrand (2005). Approximate locations of analyzed samples shown by numbered stars. More precise locations given in Table 1. ED-I is El Dorado-Introducción greenstone belt.

and intercalated intermediate to mafic tuffs, intrusions, and lavas (Fig. 3j). In places, polymictic breccia and conglomerate dominate the section (Fig. 3k). Foliation is crudely parallel to bedding except in the axial zones of folds. At least two sets of regional folds pre-date the deposition of 1.87 Ga sedimentary rocks of the Roraima group: a WNW-to W trending set and a northerly trending set.

3. U-Pb geochronology

Zircons from Paleoproterozoic rocks are commonly characterized by lead-loss, which may compromise the accuracy and decreases the precision of calculated dates. The chemical abrasion technique or CA-TIMS (Mattinson, 2005), greatly improves our ability to isolate closed-system domains of zircon for analysis. This technique, in conjunction with improved laboratory blanks, enables us to produce weighted mean $^{207}\text{Pb}/^{206}\text{Pb}$ dates with uncertainties of about 1 Ma or less, which provides sufficient resolution to test tectonic models involving Paleoproterozoic orogenic belts.

On a Concordia diagram, CA-TIMS zircon analyses typically form coherent clusters in which most of the scatter can be explained by analytical uncertainties alone. In Fig. 5, we report the uncertainties associated with the weighted mean $^{207}\text{Pb}/^{206}\text{Pb}$ dates as $\pm X/Y/Z$, where X is the internal (analytical) uncertainty, Y reflects addition of tracer uncertainty, and Z includes errors of the decay constant uncertainties (Jaffey et al., 1971). The first reported uncertainty is used when comparing to other $^{207}\text{Pb}/^{206}\text{Pb}$ dates, and the third when comparing to dates from other isotopic systems (for example, $^{40}\text{Ar}-^{39}\text{Ar}$). Although the data are plotted in Fig. 5, for these $^{207}\text{Pb}/^{206}\text{Pb}$

dates, tracer calibration contributes little to uncertainty so for simplicity we will only use internal uncertainties (x) in the text.

The U-Pb data in this paper (Table 1) were collected at the Massachusetts Institute of Technology (MIT) Isotope Lab in 2009–2010. Zircons were separated from crushed samples by standard Wilfley table, magnetic and heavy liquid techniques. Zircons were then pretreated using a modification of Mattinson's (2005) CA-TIMS technique. Methods of dissolution and digestion methodology were as described in Hoffman et al. (2011).

Pretreated grains were spiked with a mixed $^{205}\text{Pb}-^{233}\text{U}-^{235}\text{U}$ tracer solution and dissolved in HF. Dissolved Pb and U were separated using an HCl-based ion exchange procedure (modified after Krogh, 1973); loaded onto single, degassed Re filaments together with a silica gel-H $^{3}\text{PO}_4$ emitter; and their isotopic compositions measured on the VG Sector 54 thermal ionization mass spectrometer (TIMS) at MIT. Isotopic data along with details of fractionation and blank corrections appear in Table 1. The U-Pb data reduction and uncertainty propagation were done with U-Pb_Redux (Bowring et al., 2011; McLean et al., 2011) using the U decay constants of Jaffey et al. (1971) and the recommended $^{238}\text{U}/^{235}\text{U}$ of Hiess et al. (2012). Isotopic data are plotted on standard Concordia diagrams (Figs. 4 and 5).

4. Results

Samples RSH-002 and WDV-89-12 are of siliceous volcanic rocks from the Pastora terrane. WDV-89-12, a metadacitic tuff, was collected by staff of the USGS during their cooperative study of Venezuelan metallogeny and originally dated by Richard Tosdal to be 2131 ± 10 Ma (Day et al., 1995). Tosdal provided additional zircons, which we treated and analyzed

using the CA–TIMS method. Both RSH-002 and WDV-89-12 contain abundant zircons that are euhedral, elongate prisms or, more rarely, ellipsoidal, ranging up to several hundred micrometers long. No obvious cores were observed with transmitted light microscopy. Under cathodoluminescence (CL), grains show fine oscillatory growth- and sector-zonation (Fig. 4) typical of magmatic zircons. The analyzed grains yield a weighted mean $^{207}\text{Pb}/^{206}\text{Pb}$ date of 2122.65 ± 0.89 Ma and 2137.6 ± 1.0 Ma respectively. Despite structural and facies complexities, sample RSH-002 appears to be located at a lower structural level in the volcanic pile than WDV-89-12, which is clearly located above a major thrust fault (Day et al., 1995).

Sample RSH-001 is from a granitic layer within a gneiss, comprising amphibolite and granitic layers (Fig. 3h), which were interpreted in the field to represent possible basement to the rocks of the Pastora supergroup, but located above the bounding basal fault. Zircons from the sample RSH-001 are typically blocky and euhedral with prismatic and pyramidal facets. Back-scattered electron imaging of the grains (Fig. 4) revealed that they are dominantly corroded inside a narrow boundary zone and are now a spongy microgranular aggregate of fine-grained mineral phases. Similar textures were described and interpreted by Geisler et al. (2007) to indicate metasomatic replacement. Energy-dispersive X-ray measurements (EDS) of the crystals from RSH-001 showed zones of variable Zr, Si, and Ca enrichment, which are interpreted to represent recrystallization into different minerals. Moreover, inclusions of recognizable plagioclase feldspar were found in some grains. Despite chemical abrasion four analyses yielded a discordant array characterized by high common Pb (Pbc) contents and a corresponding, relatively imprecise, upper intercept date of 2146 ± 13 Ma (MSWD = 2.3). The common Pb and residual Pb-loss is likely due to incomplete removal of the damaged and/or recrystallized parts of the grains.

The occurrence of the high common Pb component in the zircons of sample RSH-001 is attributed to metasomatic alteration and recrystallization. In some cases, zircon is modified by reaction with certain kinds of hydrous fluid (e.g. Geisler et al., 2007). The Ca-enriched domains are characteristic of the presence of porous microgranular volumes associated with coupled dissolution–precipitation, where U-, Th-, and Y-rich zircon, metastable in the presence of a fluid, are recrystallized to mixtures of zircon plus other minerals, such as thorite, xenotime, and keiviite (Geisler et al., 2007), which can contain both common and radiogenic Pb. In addition to the incorporation of phases with high common Pb, the crystal lattice would have been substantially damaged so that it dissolved rapidly during the leaching process used in the CA–TIMS technique. As pointed out by Mattinson (2011) and Corfu (2013), the method works the best if the zircon grains include some regions with undamaged crystal structure so that they remained closed systems. Because of the inferred damage to the crystal lattices of zircons within sample RSH-001, we shortened the leach times; but even then – while some zircon survived – apparently not all the high Pbc inclusions in the microgranular areas were removed. Although the timing of magmatic zircon growth in the sample RSH-001 is imprecise because of the discordant grains, we consider the upper intercept date as a reliable estimate of the crystallization age and demonstrates that zircons from the sample are significantly older than zircons from the other samples of the Supamo complex.

Three widely separated samples of layered and foliated granitic gneiss from the Supamo terrane were collected as RSH-003, RSH-004 and RSH-006 (Fig. 3i). The CL images of zircons (Fig. 4) from samples RSH-004 and RSH-006 show closely spaced oscillatory zonation

indicative of magmatic crystallization. Zircons from sample RSH-003 are similarly zoned, but also contain domains with obvious signs of recrystallization and subsolidus modification as described by Corfu et al. (2003). Analysis of zircons from all three samples yield concordant clusters with weighted mean $^{207}\text{Pb}/^{206}\text{Pb}$ ages of 2108 ± 4.9 Ma, 2127.6 ± 1.3 Ma, and 2132 ± 0.49 Ma, respectively, interpreted to represent crystallization ages for the protoliths.

Another sample, RSH-005, collected from a non-penetratively deformed quartz diorite pluton, one of a larger suite of bodies interpreted in the field to be the youngest rock suite of the area, contains abundant 100–220 μm long, mostly transparent, slightly yellow, idiomorphic and short-prismatic zircons. CL images (Fig. 4) of the grains show well-developed oscillatory zoning and are interpreted as magmatic in origin. The obtained isotopic analyses cluster on Concordia and yield a weighted mean $^{207}\text{Pb}/^{206}\text{Pb}$ date of 2092 ± 1.1 Ma, consistent with their field interpretation as the youngest rocks of the area.

5. Discussion

5.1. Regional implication

As can be readily seen from the data (Figs. 5 and 6), magmatic ages from the Supamo gneisses are as young as 2108 ± 4.9 Ma and therefore their deformation was later. As the El Miamo quartzite sits unconformably upon the gneisses and does not contain the penetrative deformation characteristic of the gneisses, except for the few meters adjacent to the mylonitic shear zone, where it is strongly lineated, it is even younger. As both samples of volcanic rock from the Pastora terrane are older than the quartzite, yet sit atop them, they display “older-over-younger” relations and must have been emplaced tectonically as indicated by the mylonite beneath them. Additionally, the two volcanic samples appear to display older over younger relations.

These results have several implications. First, and as noted by Hildebrand (2005), the recognition that quartzites of the El Miamo formation sit atop both the Imataca and Supamo terranes indicates that, if it is the same quartzite unit, the two were joined prior to deposition of the quartzite. Second, the main deformational event of the region is the emplacement of Pastora allochthons atop the quartzite and its basement. This age of this event is poorly constrained, but it must be younger than the youngest rocks involved, which are $\sim 2108 \pm 4.9$ Ma and older than the unconformably overlying 1.87 Roraima supergroup (Santos et al., 2003). If the non-penetratively deformed quartz dioritic pluton (RSH-005) postdates the deformation, which is unclear as they weren't observed to cut the fault or rocks of the Pastora allochthon, it would place an upper limit on the age of thrusting as 2092 ± 1.1 Ma. This solution would leave about 16 Myr for deformation of the Supamo rocks, erosion and deposition of the quartzite, emplacement of the Pastora allochthon at 2100 ± 8 Ma, and intrusion of the post-kinematic diorite bodies.

Our data fit well with ages of 2120 ± 2 Ma for a foliated siliceous volcanic rock and 2094 ± 1 Ma for a post-deformational diorite, in the Barama-Mazaruni belt in Guyana (Norcross et al., 2000). The author has examined the western margin of this belt in Venezuela, where it is called the El Dorado-Introducción (Fig. 2), and found the quartzite and the basal thrust between the Pastora greenstones and Supamo gneisses, so it is likely that rocks in this belt are also part of the Pastora allochthon. Similarly, in the correlative Birimian greenstone belts of West Africa, Davis et al. (1994) dated a post-kinematic pluton at 2090 ± 1 Ma whereas detrital zircons from volcanogenic sediments – no younger

Fig. 3. a. Detail of bedded quartzite; b. the quartzite is commonly disaggregated due to the deep tropical weathering of the subjacent Supamo gneisses; c. strip-mining the quartzite for iron smelters; d. typical view of small artisanal quarries in the mylonite; e. detailed view of mylonite showing incorporated phacoids of gneiss; f. extremely attenuated folds in metabasalt above basal mylonite and beneath much less deformed and recognizable pillow lavas; g. scenic view showing the differences in topography and vegetation between the Pastora supergroup, which forms forested hills, and rocks of the Supamo terrane, which are chemically weathered and support only grasses, sedges, and sparse trees typical of a savanna, or llano, environment; h. low grade and non-penetratively deformed pebbly conglomerate with ashstone rip-ups of the Pastora supergroup; i. saprolitic debris flow deposit of the Pastora supergroup; j. intercalated amphibolite and granitic orthogneiss, interpreted to represent basement to the Pastora supergroup as it occurs above the quartzite and basal mylonite; and k. foliated orthogneiss of the Supamo complex.





Fig. 3 (continued).

Table 1
Data table for analyses. Locations of samples are listed and datum is Prov. South Amer. 56, zone 20 N.

Fraction	Composition		Isotopic ratios								Dates [Ma]						Corr. coef.	
	Th/U ^a	Pbc ^b [pg]	Pb ⁸⁷ /Pbc ^c	²⁰⁶ Pb/ ²⁰⁴ Pb ^d	²⁰⁸ Pb/ ²⁰⁶ Pb ^e	²⁰⁶ Pb/ ²³⁸ U ^{e,f}	±2σ [%]	²⁰⁷ Pb/ ²³⁵ U ^e	±2σ [%]	²⁰⁷ Pb/ ²⁰⁶ Pb ^{e,f}	±2σ [%]	²⁰⁶ Pb/ ²³⁸ U ^{g,h}	±2σ [abs.]	²⁰⁷ Pb/ ²³⁵ U ^g	±2σ [abs.]	²⁰⁷ Pb/ ²⁰⁶ Pb ^{g,h}		±2σ [abs.] ^h
RSH-001: Zircon	613747, 855392		Gneiss															
z7	0.05	4.8	4.76	320.3	0.015	0.096658	0.24	1.73446	1.17	0.130204	1.138	594.8	1.4	1021.4	7.57	2099.92	20.0	0.25
z8	0.06	9.1	4.23	286.5	0.018	0.090570	0.27	1.59501	1.34	0.127784	1.299	558.9	1.4	968.3	8.35	2066.92	22.9	0.25
z9	0.10	37.5	5.41	356.1	0.031	0.193944	0.30	3.50506	1.05	0.131133	0.987	1142.7	3.2	1528.4	8.31	2112.41	17.3	0.35
z10	0.12	93.6	9.27	594.9	0.034	0.227985	0.16	4.17345	0.61	0.132826	0.575	1323.9	1.9	1668.8	4.98	2134.87	10.1	0.33
RSH-002: Zircon	598239, 832154		Metatuff															
z3	0.77	0.9	64.07	3457.8	0.219	0.390017	0.11	7.08726	0.18	0.131852	0.110	2122.9	1.9	2122.4	1.57	2122.00	1.9	0.80
z4	0.77	0.6	85.80	4625.5	0.219	0.390306	0.14	7.09548	0.18	0.131908	0.104	2124.2	2.5	2123.5	1.63	2122.73	1.8	0.82
z5	0.77	0.8	89.36	4816.6	0.219	0.389090	0.10	7.07228	0.16	0.131887	0.107	2118.6	1.9	2120.6	1.44	2122.46	1.9	0.75
z6	0.76	1.1	56.95	3080.3	0.217	0.390279	0.10	7.09659	0.17	0.131938	0.108	2124.1	1.9	2123.6	1.52	2123.13	1.9	0.80
z7	0.78	1.0	63.99	3441.8	0.224	0.389626	0.06	7.08288	0.15	0.131904	0.149	2121.1	1.0	2121.9	1.32	2122.67	2.6	0.17
RSH-003: Zircon	718914, 829801		Gneissic granite unconformably beneath quartzite															
z1	0.81	2.4	16.61	900.2	0.231	0.394731	0.30	7.28790	0.49	0.133966	0.388	2144.7	5.4	2147.3	4.41	2149.82	6.8	0.62
z4	0.09	1.4	5.43	359.0	0.027	0.387444	0.86	6.99664	1.35	0.131031	1.032	2111.0	15.4	2111.0	12.02	2111.04	18.1	0.65
z6	0.45	1.2	9.94	591.4	0.128	0.387336	0.24	6.99706	0.67	0.131076	0.615	2110.5	4.3	2111.1	5.99	2111.64	10.8	0.41
z7	0.26	0.9	7.74	484.0	0.075	0.386912	0.46	6.97764	0.90	0.130855	0.720	2108.5	8.2	2108.6	7.95	2108.68	12.6	0.60
z8	0.24	0.7	12.76	790.2	0.069	0.385960	0.28	6.95517	0.54	0.130755	0.462	2104.1	5.0	2105.7	4.82	2107.35	8.1	0.52
z10	0.40	1.0	9.90	596.2	0.113	0.385017	0.56	6.93490	1.00	0.130694	0.632	2099.7	10.0	2103.1	8.84	2106.52	11.1	0.81
RSH-004: Zircon	586726, 801399		Layered granitic gneiss															
z3	0.79	1.3	9.69	535.9	0.225	0.390658	0.18	7.12875	0.68	0.132407	0.623	2125.9	3.2	2127.6	6.04	2129.34	10.9	0.43
z4	0.82	1.0	55.69	2972.8	0.235	0.391002	0.36	7.12790	0.38	0.132275	0.107	2127.5	6.6	2127.5	3.42	2127.59	1.9	0.96
z6	0.38	0.7	58.62	3449.9	0.107	0.390156	0.38	7.11118	0.41	0.132251	0.132	2123.6	6.8	2125.4	3.61	2127.28	2.3	0.95
z8	0.41	1.3	67.25	3926.1	0.116	0.389865	0.51	7.10742	0.53	0.132279	0.146	2122.2	9.2	2125.0	4.76	2127.66	2.6	0.96
RSH-005: Zircon	585208, 804399		Qtz diorite															
z1	0.23	1.8	30.08	1844.6	0.065	0.384264	0.17	6.88731	0.27	0.130051	0.199	2096.2	3.0	2097.0	2.38	2097.86	3.5	0.67
z3	0.25	1.4	43.04	2616.7	0.073	0.383280	0.19	6.84688	0.24	0.129620	0.148	2091.6	3.3	2091.8	2.17	2092.02	2.6	0.80
z4	0.29	1.1	9.51	587.3	0.083	0.382565	0.48	6.81895	0.83	0.129332	0.651	2088.3	8.6	2088.2	7.34	2088.12	11.5	0.62
z7	0.29	1.0	261.41	15673.4	0.082	0.381746	0.07	6.82132	0.10	0.129655	0.092	2084.4	1.3	2088.5	0.88	2092.50	1.6	0.45
z8	0.36	1.2	35.48	2109.2	0.102	0.384653	0.24	6.87061	0.34	0.129605	0.218	2098.0	4.3	2094.9	2.99	2091.82	3.8	0.76
z9	0.39	0.7	126.51	7423.6	0.110	0.383320	0.18	6.84991	0.22	0.129663	0.106	2091.8	3.2	2092.2	1.99	2092.62	1.9	0.88
RSH-006: Zircon	604567, 799094		Layered granitic gneiss															
z1	0.37	1.0	95.56	5612.6	0.107	0.393151	0.27	7.19630	0.29	0.132814	0.086	2137.4	4.8	2136.0	2.57	2134.71	1.5	0.95
z2	0.38	1.8	143.06	8383.9	0.108	0.391969	0.12	7.17846	0.12	0.132884	0.076	2132.0	2.2	2133.8	1.11	2135.64	1.4	0.80
z3	0.25	1.2	291.97	17640.0	0.070	0.391317	0.07	7.15239	0.10	0.132622	0.049	2128.9	1.2	2130.6	0.89	2132.19	0.9	0.89
z4	0.30	1.0	668.30	39843.6	0.085	0.391130	0.08	7.15224	0.11	0.132683	0.052	2128.1	1.4	2130.6	1.00	2132.99	0.9	0.90
z5	0.33	0.6	333.88	19755.3	0.095	0.392392	0.07	7.17514	0.12	0.132679	0.063	2133.9	1.3	2133.4	1.05	2132.94	1.1	0.87
z7	0.34	1.3	385.76	22763.2	0.098	0.390409	0.12	7.13286	0.14	0.132568	0.058	2124.7	2.1	2128.2	1.22	2131.47	1.0	0.90
z8	0.34	2.3	233.41	13780.1	0.098	0.392153	0.09	7.17323	0.12	0.132725	0.055	2132.8	1.6	2133.2	1.09	2133.54	1.0	0.90
WDV-89-12: Zircon	Day et al. (1995)		Metatuff															
z1	0.67	0.9	34.79	1926.0	0.190	0.393045	0.38	7.20323	0.44	0.132978	0.217	2136.9	7.0	2136.9	3.89	2136.87	3.8	0.87
z2	0.59	0.4	95.85	5362.3	0.168	0.392071	0.33	7.18952	0.35	0.133054	0.151	2132.4	6.0	2135.2	3.08	2137.88	2.7	0.90
z3	0.74	1.0	65.48	3554.7	0.210	0.391221	0.20	7.17443	0.23	0.133064	0.119	2128.5	3.7	2133.3	2.08	2138.00	2.1	0.86
z7	0.71	0.3	87.57	4777.0	0.202	0.392350	0.37	7.18749	0.40	0.132922	0.132	2133.7	6.7	2135.0	3.55	2136.14	2.3	0.94
z8	0.59	0.9	68.42	3833.5	0.168	0.391835	0.21	7.18384	0.29	0.133029	0.163	2131.3	3.9	2134.5	2.57	2137.55	2.9	0.83
z9	0.61	1.2	63.63	3547.6	0.175	0.392610	0.41	7.19998	0.44	0.133065	0.112	2134.9	7.4	2136.5	3.90	2138.02	2.0	0.97

Blank and oxygen composition: ²⁰⁶Pb/³³⁴Pb = 18.42 ± 0.35; ²⁰⁷Pb/²⁰⁴Pb = 15.35 ± 0.23; ²⁰⁸Pb/²⁰⁴Pb = 37.46 ± 0.74; ¹⁸O/¹⁶O = 0.00205 ± 0.00002.

corr. coef. = correlation coefficient locations.

^a Th contents calculated from radiogenic ²⁰⁸Pb and the ²⁰⁷Pb/²⁰⁶Pb date of the sample, assuming concordance between U-Th and Pb systems.

^b Total mass of common Pb.

^c Ratio of radiogenic Pb (including ²⁰⁸Pb) to common Pb.

^d Measured ratio corrected for fractionation and tracer contribution only.

^e Measured ratios corrected for fractionation, tracer, blank, common Pb is lab blank, U blank = 0.1 pg; mass fractionation correction of 0.25‰/amu ± 0.04‰/amu (atomic mass unit) was applied to single-collector Daly measurements.

^f Corrected for initial Th/U disequilibrium using radiogenic ²⁰⁸Pb and Th/U [magma] = 2.8.

^g Isotopic dates calculated using the decay constants A238 = 1.55125E - 10 yr⁻¹, A235 = 9.8485E - 10 yr⁻¹ (Jaffey et al., 1971), and for the ²³⁸U/²³⁵U = 137.818 ± 0.045 (Hiess et al., 2012).

^h Fraction excluded from age calculation.

than 2116 ± 2 Ma, the age of a pluton that intrudes them – derived from the nearby volcanics and comagmatic plutons yielded ages ranging from 2184 to 2132 ± 5 Ma, which serve to bracket the age of deformation between about 2132 and 2090 Ma. Thus, ages in all three areas support major deformation at about 2100 Ma.

The Pastora allochthon contains a wide variety of volcanic and sedimentary rocks in several thrust sheets. The lower thrust sheets are dominated by massive and pillowed basalt-basaltic andesitic lavas and breccias structurally overlain by intermediate-siliceous fragmental rocks, including ignimbrite and a variety of volcanoclastic rocks. Small mafic and intermediate composition plutons intruded the volcanic and associated rocks prior to thrusting. Based on compositions and eruptive styles, Hildebrand (2005) suggested that the rocks of the allochthon most likely represent the rocks of a dismembered magmatic arc. It is possible that the quartzite represents the basal part of passive margin sequence remaining beneath the detachment. If correct, the allochthons would have been emplaced during arc-continent collision.

Overall, the cusped form of the granite–greenstone terrane is not the result of intrusion by domical-shaped intrusions rising diapirically into the volcano-sedimentary pile as originally envisioned by Macgregor (1951) for granite–greenstones in Zimbabwe, and still a popular explanation for pluton emplacement (Hickman, 1984; Bateman, 1992; Pitcher, 1993; Paterson and Vernon, 1995; Saleeby, 1999; Van Kranendonk et al., 2004); instead, the cusped form represents the tectonic juxtaposition of rocks of the Pastora supergroup above rocks of the Supamo terrane followed by two periods of large-scale regional folding. Folds can readily be delineated within the supracrustal rocks but due mainly to lack of exposure are impossible to resolve in the Supamo complex. A few synclinal remnants of the quartzite within the gneiss complex were identified during mapping and further attest to the folded nature of the complex. Similar interference patterns are common in Precambrian rocks of the Canadian Shield (Hoffman, 1988), in other cratons such as the Zimbabwe (Snowden and Bickle, 1976; Snowden, 1984) and Yilgarn (Platt, 1980; Myers and Watkins, 1985),

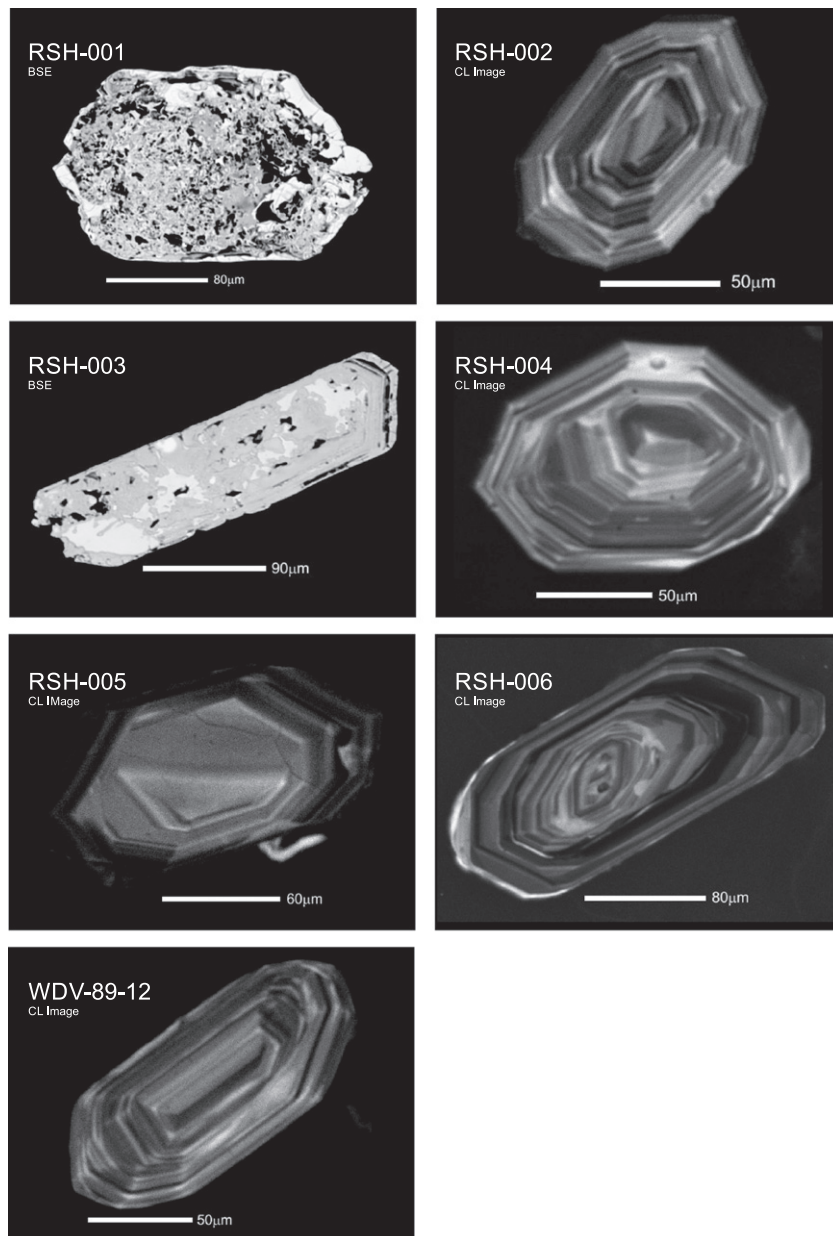


Fig. 4. Backscatter-electron and cathodoluminescence images of representative zircons from each sample dated in this study.

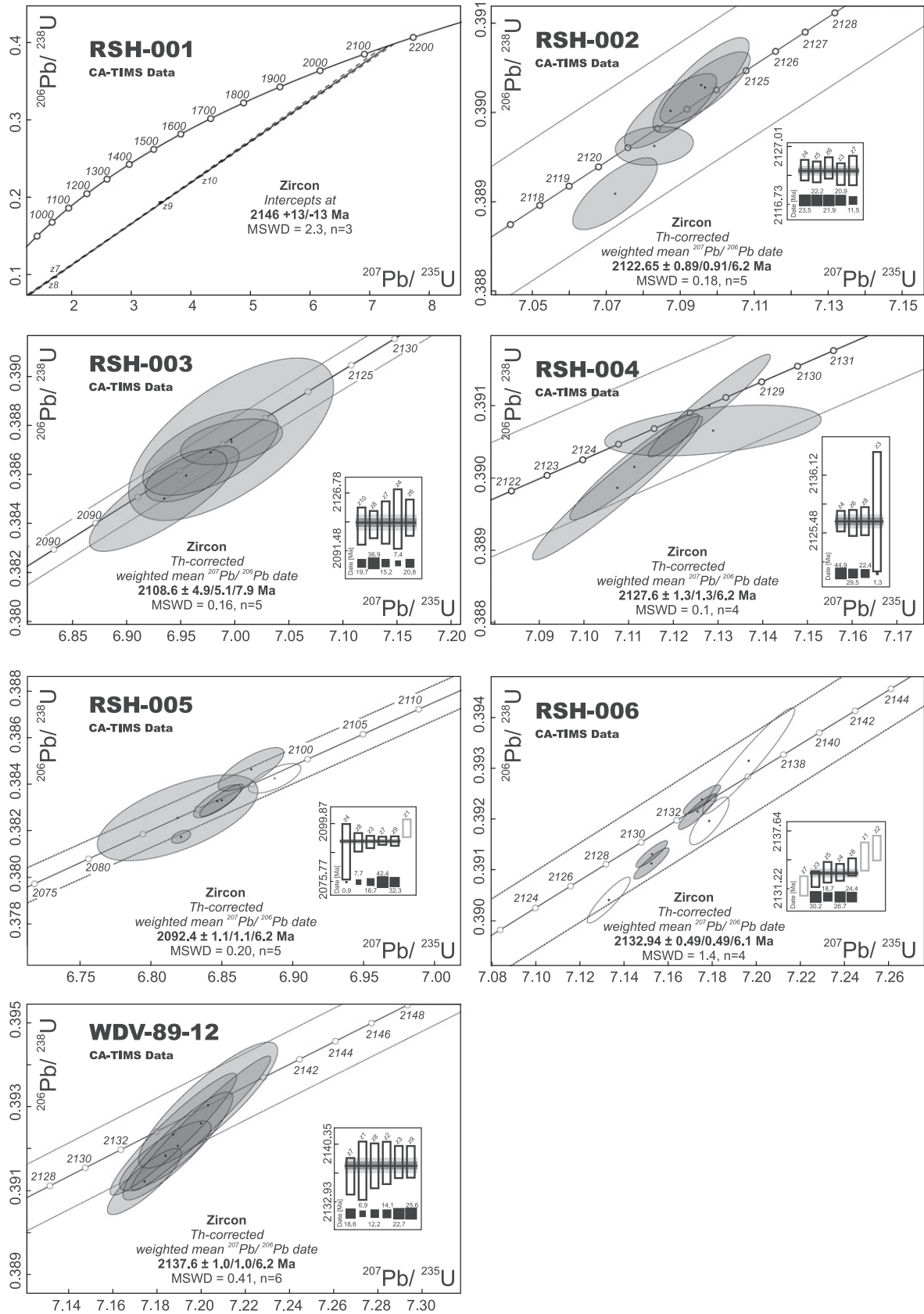


Fig. 5. U–Pb zircon ages for samples from the Guayana shield analyzed in this study.

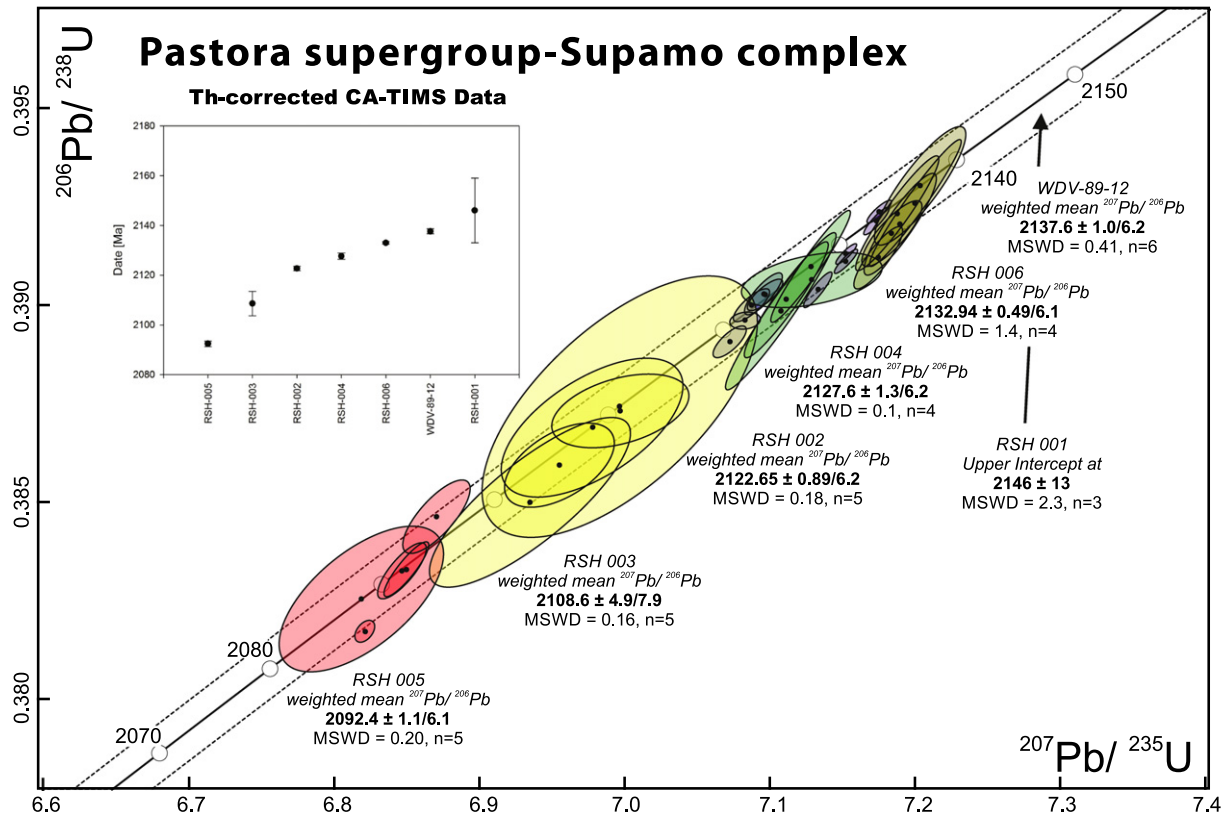


Fig. 6. U–Pb zircon ages for samples from the Guayana shield analyzed in this study.

and even within the Cretaceous Sierra Nevada of California (see figure 46 of Hildebrand, 2013).

Based on our field mapping and U–Pb geochronology we conclude that rocks of the Supamo complex did not intrude rocks of the Pastora and instead the relationship between the two is entirely tectonic as originally suggested by Hildebrand (2005). Thus, the overall map pattern of the Guayana shield is mainly due to the several periods of deformation: (1) subduction of the Supamo terrane beneath Pastora terrane and emplacement of the Pastora allochthon followed by (2) two periods of younger folding to create the dome and basin interference pattern readily visible on the regional maps.

Numerous active and inactive gold mines occur throughout the greenstone belts. The gold occurs in brittle to ductile fault zones as native gold, commonly visible in drill core, and as microinclusions within pyrite. Using mapped relations in the El Callao area, Hildebrand (2005) showed that the mineralized faults were truncated by regional folded thrust faults, which – because they are continuous along strike for many kilometers, are gently inclined with respect to bedding, and folded along with the strata – he reasoned likely formed during imbrication of the Pastora allochthon, and thus predated the two periods of late folding. He exploited these relationships to restore the mineralized faults to their pre-folding orientations and showed that the auriferous faults were originally normal faults, not the reverse faults observed today. The data presented here confirm his model, which implies that the gold mineralization predates emplacement of the Pastora allochthon. This largely precludes gold mineralization in the Supamo complex, which is consistent with observations (Orris et al., 1993).

5.2. Nature of greenstone belts

We think that the geological relationships documented here are worth placing in context with other models for the origin and development of greenstone belts. For decades, many geologists

considered greenstone belts to be fill of autochthonous rift basins formed upon older continental crust (Hunter, 1974; Baragar and McGlynn, 1976; Goodwin, 1977; Archibald et al., 1978; Kröner, 1981; Leube et al., 1990; Bleeker, 2002). However, we now understand that greenstone belts are erosional remnants of formerly more extensive, structurally complex, and compositionally diverse domains that owe their distinctive outcrop patterns largely to the rheological difference between layered sedimentary and volcanic rocks and more massive crystalline rocks, such as plutons and gneisses, during deformation. Below we mention a few well-studied and/or innovative, examples to illustrate that relations in the Guayana shield are similar to those in many greenstone belts of other cratons.

In a prescient overview, Folinsbee et al. (1968) argued that Archean greenstones capped by dacitic lavas in the Slave province of northwestern Canada represented arc magmatism, but were seemingly unrelated to the Neoproterozoic granitic rocks beneath them. Later, Kusky (1989) interpreted rocks in the Slave province to represent the accretion of the Neoproterozoic Hackett River arc and accretionary prism to the much older Anton terrane located in the western Slave province. Hoffman (1991), utilizing examples from the Canadian shield, suggested that greenstone belts were dominantly allochthonous with respect to their underlying basement, and presented a general accretionary model for their origin that successfully explained the diversity of rock types and structural histories.

In the central Superior Province of Canada, rocks of the Wawa-Abitibi greenstone belt contain recumbent folds and are widely interpreted to represent Mesoproterozoic arc terranes thrust over rocks of the similar-age Pontiac belt (McGill and Shradly, 1986; Percival et al., 2012). Farther west at Steep Rock Lake, an assemblage of structurally overturned mafic lavas, sills and associated metasedimentary rocks were thrust over a 3.0 Ga tonalitic basement complex and its unconformably overlying passive margin sequence comprising basal siliciclastics and a paleokarst-capped carbonate platform (Hoffman, 1991; Kusky and Hudleston, 1999).

Within the Trans-Hudson orogen of the west-central Canadian Shield, 3.12 Ga crystalline basement and 2.40 Ga plutons of the Sask craton were overthrust, at about 1.82 Ga, by an amphibolite-grade assemblage of arc volcanics, metasedimentary rocks and plutons (Ashton et al., 2005). In the northeastern Canadian Shield, 2.0 Ga tholeiites and ultramafic rocks of the Cape Smith Belt, interpreted to represent the floor of a collapsed ocean basin and 1.9–1.86 Ga arc, were thrust over Neoproterozoic basement gneisses of the northeastern Superior province, and their overlying passive margin rocks, at about 1.87 Ga (Hoffman, 1985; St-Onge et al., 1992).

In the 3.5–3.3 Ga Barberton greenstone belt of Kaapvaal craton, Lamb (1987) showed that thrusts and sedimentary rocks were similar to Quaternary thrusts and accretionary prism sediments of coastal New Zealand, and Schoene et al. (2008) suggested that the belt was accreted during a period of oblique convergence at about 3.23 Ga. In the Zimbabwe craton, Kusky (1998) explored the geology of several greenstone belts and found that two similar-age magmatic belts, each composed of several individual belts, have different rock suites, geochemistry and relations to surrounding rocks such that one could readily be interpreted as an autochthonous magmatic arc and the other as an allochthonous arc thrust over the craton. Furthermore, Hofmann et al. (2001) showed that one package of 2.65 Ga sedimentary rocks in the Belingwe greenstone belt of Zimbabwe could be logically interpreted as imbricated foredeep fill.

In the Yilgarn craton of Australia >2.9 to 2.7 Ga tholeiites and calc-alkaline volcanic rocks of the Norseman–Wiluna belt were recumbently folded, involved in thin skin thrusting, and provided detritus for a contemporaneous foredeep basin at around 2.69 Ga (Barley and Groves, 1990). Myers and Watkins (1985) argued that the rocks of the Yilgarn greenstone belts and younger gneisses were involved in thrust regime and were later intruded by sheet-like plutons of monzogranite before being folded into a dome and basin interference pattern by two deformational events.

As stated earlier, the 2.1 Ga greenstone belts of the Guayana shield were generally considered to be autochthonous basins intruded and metamorphosed by younger plutons (Mendoza, 1977; Cox et al., 1993). Here we demonstrated that the ages of the rocks are incompatible with such a model; instead they support the Hildebrand (2005) model in which a telescoped arc was thrust onto another terrane, which contained both older and younger rocks. Likewise, Davis et al. (1994) interpreted correlative rocks in the Birimian of West Africa to represent arc and subjacent accretionary complexes.

In each belt one or two subsequent deformational events created complex dome- and basin-type interference patterns involving basement, greenstones and younger plutons (for example: Snowden and Bickle, 1976; Snowden, 1984; Myers and Watkins, 1985). The younger folds are beneficial and highly exploitable because geological maps provide oblique down-plunge views through the belts (Stockwell, 1950).

Despite their differences in age, detailed stratigraphy, and compositions, these highlighted examples show a similar geological history and are inconsistent with simple basinal models for the origin of greenstone belts. A recurrent theme is the emplacement of volcano-plutonic allochthons over continental crust as shown here for the Guayana shield.

Acknowledgments

Richard Tosdal is thanked for providing additional zircon separates. Alejandro “Cachete” Guerrero, our Venezuelan field assistant, cheerfully assisted with the fieldwork in every way possible. We thank Henry Sanchez of Tumeremo for assistance. Comments by Clark Isachsen and an anonymous reviewer helped to improve the paper.

References

- Angel, Karen, 2012. Why the world's tallest waterfall is named Angel Falls. *Terrae Incognitae* 44 (1), 16–42.
- Archibald, N.J., Bettenay, L.F., Binns, R.A., Groves, D.I., Gunthorpe, R.J., 1978. The evolution of Archean greenstone terrains, Eastern Goldfield Province, Western Australia. *Precambrian Research* 9, 103–132.
- Ashton, K.E., Lewry, J.F., Heaman, L.M., Hartlaub, R.P., Stauffer, M.R., Tran, H.T., 2005. The Pelican Thrust Zone: basal detachment between the Archean Sask Craton and Paleoproterozoic Flin Flon–Glennie Complex, western Trans-Hudson Orogen. *Canadian Journal of Earth Sciences* 42, 685–706.
- Baragar, W.R.A., McGlynn, J.C., 1976. Early Archean basement in the Canadian Shield: a review of the evidence. *Geological Survey of Canada, Paper* 76–14.
- Barley, M.E., Groves, D.I., 1990. Deciphering the tectonic evolution of Archean greenstone belts: the importance of contrasting histories to the distribution of mineralization in the Yilgarn Craton, Western Australia. *Precambrian Research* 46, 3–20.
- Bateman, P.C., 1992. Plutonism in the Central Part of the Sierra Nevada Batholith, California: United States. *United States Geological Survey Professional Paper* 1483 (186 pp.).
- Bleeker, W., 2002. Archean tectonics: a review, with illustrations from the Slave craton. In: Fowler, C.M.R., Ebinger, C.J., Hawkesworth, C.J. (Eds.), *The Early Earth: Physical, Chemical, and Biological Development*. Geological Society, London, Special Publications, 199, pp. 151–181.
- Bowring, J.F., McLean, N.M., Bowring, S.A., 2011. Engineering cyber infrastructure for U–Pb geochronology: Tripoli and U–Pb_Redux. *Geochemistry, Geophysics, Geosystems* 12, Q0AA19.
- Cordani, U.G., Teixeira, W., 2007. Proterozoic accretionary belts in the Amazonian Craton. In: Hatcher, R.D., Carlson, M.P., McBride, J.H., Martinez, C. (Eds.), *4-D Framework of Continental Crust*. Geological Society of America Memoir, 200, pp. 297–320.
- Corfu, F., 2013. A century of U–Pb geochronology: the long quest towards concordance. *Geological Society of America Bulletin* 125, 33–47.
- Corfu, F., Hanchar, J.M., et al., 2003. Atlas of Zircon Textures. *Reviews in Mineralogy and Geochemistry* 53, 469–500.
- Cox, D.P., Wynn, J.C., Sidder, G.B., Page, N.J., 1993. Geology of the Venezuelan Guayana shield. *U.S. Geological Survey and Corporacion Venezolana de Guayana, Tecnica Minera, C.A., Geology and Mineral Resource Assessment of the Venezuelan Guayana shield*. U.S. Geological Survey Bulletin, 2062, pp. 9–15.
- Davis, D.W., Hirdes, W., Schaltegger, U., Nunoo, E.A., 1994. U–Pb age constraints on deposition and provenance of Birimian and gold-bearing Tarkwaian sediments in Ghana, West Africa. *Precambrian Research* 67, 89–107.
- Day, W.C., Tosdal, R.M., Acosta, E.L., Aruspon, J.C., Carvajal, L., Cedeño, E., Lowry, G., Martinez, L.F., Noriega, J.A., Nuñez, F.J., Rojas, J., Prieto, F., 1995. Geology of the Lo Increible mining district and U–Pb age of the early Proterozoic Yuruari Formation of the Pastora Supergroup, Guayana shield. *Geology and Mineral Deposits of the Venezuelan Guayana Shield*. U.S. Geological Survey Bulletin, 2124, pp. E1–E13.
- Dougan, T.W., 1977. The Imataca Complex near Cerro Bolivar, Venezuela — a calc-alkaline Archean protolith. *Precambrian Research* 4, 237–268.
- Doyle, A.C., 1912. *The Lost World*. Hodder & Stoughton, New York (309 pp.).
- Folinsbee, R.E., Baadsgaard, H., Cumming, G.L., Green, D.C., 1968. A Very Ancient Island Arc. In: Knopoff, L., Drake, C.L., Ehart, P.J. (Eds.), *The Crust and Upper Mantle of the Pacific Area*. *Geophys. Monogr. Ser.*, vol. 12. AGU, Washington, D. C., pp. 441–448.
- Geisler, T., Schaltegger, U., Tomaschek, F., 2007. Re-equilibration of zircon in aqueous fluids and melts. *Elements* 3, 43–50.
- Gleason, H.A., Killip, E.P., 1938. The Flora of Mount Auyan-Tepui, Venezuela. *Brittonia* 3, 141–204.
- Goodwin, A.M., 1977. Archean basin–craton complexes and the growth of Precambrian shields. *Canadian Journal of Earth Sciences* 15, 2737–2759.
- Haines, T., 2004. Seeking Heaven in the Stubborn Earth. *Boston Globe* M1–M8 (September 26).
- Hickman, A.H., 1984. Archean diapirism in the Pilbara Block, Western Australia. In: Kröner, A., Greiling, R. (Eds.), *Precambrian Tectonics Illustrated*. Schweizerbart'sche Verlagsbuchhandlung, Stuttgart, pp. 113–127.
- Hiess, J., Condon, D.J., McLean, N., Noble, S.R., 2012. ²³⁸U/²³⁵U systematics in terrestrial uranium minerals. *Science* 335, 1610–1614.
- Hildebrand, R.S., 2005. Autochthonous and allochthonous strata of the El Callao greenstone belt: implications for the nature of the Paleoproterozoic Trans-Amazonian orogeny and the origin of gold-bearing veins in the El Callao mining district, Guayana shield, Venezuela. *Precambrian Geology* 143, 75–86.
- Hildebrand, R.S., 2013. Mesozoic Assembly of the North American Cordillera. *Geological Society of America, Special Paper* 495, 169p.
- Hoffman, P.F., 1985. Is the Cape Smith Belt (northern Quebec) a klippe? *Canadian Journal of Earth Sciences* 22, 1361–1369.
- Hoffman, P.F., 1988. United Plates of America, The Birth of a Craton: Early Proterozoic assembly and growth of Laurentia. *Annual Review of Earth and Planetary Sciences* 16, 543–603.
- Hoffman, P.F., 1991. On accretion of granite–greenstone terranes. In: Sheahan, R.F., P.A., Green, S.B. (Eds.), *Greenstone Gold and Crustal Evolution*. Geological Association of Canada, St. John's, Newfoundland, pp. 32–45.
- Hoffman, P.F., Bowring, S.A., Buchwaldt, R., Hildebrand, R.S., 2011. Birthdate for the Coronation paleocean: age of initial rifting in Wopmay orogen, Canada. *Canadian Journal of Earth Sciences* 48, 281–293.
- Hofmann, A., Dirks, P.H.G.M., Jelsma, H.A., 2001. Late Archean foreland basin deposits, Belingwe greenstone belt, Zimbabwe. *Sedimentary Geology* 141–142, 131–168.
- Hunter, R.D., 1974. Crustal development of the Kaapvaal craton. I. The Archean. *Precambrian Research* 1, 259–294.
- Hurley, P.M., Fairbairn, H.W., Gaudette, H.E., 1976. Progress report on early Archean rocks in Liberia, Sierra Leone, and Guayana, and their general stratigraphic setting. In:

- Windley, B.F. (Ed.), *The Early History of the Earth*. John Wiley and Sons, New York, pp. 511–521.
- Jaffey, H., Flynn, K.F., Glendenin, L.E., Bentley, W.C., Essling, A.M., 1971. Precision measurement of half-lives and specific activities of ^{235}U and ^{238}U . *Physical Review* 4, 1889–1906.
- Korol, B., 1965. Estratigrafía de la Serie Pastora en la región Guasipati-El Dorado. *Dirección de Geología Boletín*, Caracas, vol. 7. Ministerio de Minas e Hidrocarburos, pp. 3–17.
- Krogh, T.E., 1973. A low-contamination method for hydrothermal decomposition of zircon and extraction of U and Pb for isotopic age determinations. *Geochimica et Cosmochimica Acta* 37, 485–494.
- Kröner, A., 1981. Precambrian plate tectonics: in Precambrian plate tectonics. In: Kröner, A. (Ed.), *Developments in Precambrian Geology*, 4. Elsevier, Amsterdam, The Netherlands, pp. 57–90.
- Kusky, T.M., 1989. Accretion of the Archean Slave province. *Geology* 17, 63–67.
- Kusky, T.M., 1998. Tectonic setting and terrane accretion of the Archean Zimbabwe craton. *Geology* 26, 163–166.
- Kusky, T.M., Hudleston, P.J., 1999. Growth and demise of an Archean carbonate platform, Steep Rock Lake, Ontario, Canada. *Canadian Journal of Earth Sciences* 36, 565–584.
- Lamb, S., 1987. Archean synsedimentary tectonic deformation—a comparison with the Quaternary. *Geology* 15, 565–568.
- Leube, A., Hirdes, W., Mauer, R., Kesse, G.O., 1990. The early Proterozoic Birimian Supergroup of Ghana and some aspects of its associated gold mineralization. *Precambrian Research* 46, 139–165.
- Macgregor, A.M., 1951. Some milestones in the Precambrian of Southern Rhodesia. *Transactions of the Geological Society of South Africa* 54, 27–71.
- Mattinson, J.M., 2005. Zircon U–Pb chemical abrasion (CA–TIMS) method: combined annealing and multi-step partial dissolution analysis for improved precision and accuracy of zircon ages. *Chemical Geology* 220 (1–2), 47–66. <http://dx.doi.org/10.1016/j.chemgeo.2005.03.011>.
- Mattinson, J.M., 2011. Extending the Krogh legacy: development of the CA–TIMS method for zircon geochronology. *Canadian Journal of Earth Sciences* 48, 95–105.
- McGill, G.E., Shradly, C.H., 1986. Evidence for a complex deformational history, southwestern Michipicoten greenstone belt. *Journal of Geophysical Research* 91, 281–289.
- McLean, N.M., Bowring, J.F., Bowring, S.A., 2011. An algorithm for U–Pb isotope dilution data reduction and uncertainty propagation. *Geochemistry, Geophysics, Geosystems* 12, Q0AA18.
- Mendoza, S.V., 1977. Evolución tectónica del Escudo de Guayana. Segundo Congreso Latinoamericano de Geología, Caracas, 1973. Memoria, Publicación Especial 7, vol. 3, pp. 2237–2270.
- Mendoza, S.V., 2000. Evolución geotectónica y recursos minerales del escudo de Guayana en Venezuela (y su relación con escudo Sudamericano). Instituto Geográfico de Venezuela Simón Bolívar, Ciudad Bolívar (p. 184) (in Spanish).
- Menéndez, V. de V.A., 1968. Revisión de la estratigrafía de la Provincia de Pastora según el estudio de la región de Guasipati, Guayana Venezolana. *Dirección de Geología Boletín*, Caracas, vol. 9. Ministerio de Minas e Hidrocarburos, pp. 309–338.
- Myers, J.S., Watkins, K.P., 1985. Origin of granite–greenstone patterns, Yilgarn Block, Western Australia. *Geology* 13, 778–780.
- Norcross, C., Davis, D.W., Spooner, E.T.C., Rust, A., 2000. U–Pb and Pb–Pb age constraints on Paleoproterozoic magmatism, deformation and gold mineralization in the Omai area, Guyana shield. *Precambrian Research* 102, 69–86.
- Orris, G.J., Page, N.J., Bolm, K.S., Gray, F., Brooks, W.E., Carbonaro, M.M., Kibbe, R., 1993. Mines, prospects, and occurrences of the Venezuelan Guayana shield: in *Geology and Mineral Deposits of the Venezuelan Guayana Shield*. U.S. Geological Survey Bulletin 2024, 29–53.
- Paterson, S.R., Vernon, R.H., 1995. Bursting the bubble of ballooning plutons: a return to nested diapirs emplaced by multiple processes. *Geological Society of America Bulletin* 107, 1356–1380.
- Percival, J.A., Skulski, T., Sanborn-Barrie, M., Stott, G.M., Leclair, A.D., Corkery, M.T., Boily, M., 2012. Geology and tectonic evolution of the Superior Province, Canada. In: Percival, J.A., Cook, F.A., Clowes, R.M. (Eds.), Chapter 6 In *Tectonic Styles in Canada: The LITHOPROBE Perspective*. Geological Association of Canada, Special Paper, 49, pp. 321–378.
- Pitcher, W.S., 1993. *The Nature and Origin of Granite*. Blackie Academic & Professional, London (321 pp.).
- Platt, J.P., 1980. Archean greenstone belts: A structural test of tectonic hypotheses. *Tectonophysics* 65, 127–150.
- Robertson, R., 1949. Jungle Journey to the World's Highest Waterfall: Angel Falls in Venezuela. *National Geographic* 96 (5), 635–690.
- Saleeby, J.B., 1999. On some aspects of the geology of the Sierra Nevada. In: Moores, E.M., Sloan, D., Stout, D.L. (Eds.), *Classic Cordilleran Concepts: A View From California*. Boulder, Colorado, Geological Society of America Special Paper, 338, pp. 173–184.
- Santos, J.O.S., Potter, P.E., Reis, N.J., Hartmann, L.A., Fletcher, I.R., McNaughton, N.J., 2003. Age, source, and regional stratigraphy of the Roraima Supergroup and Roraima-like outliers in northern South America based on U–Pb geochronology. *Geological Society of America Bulletin* 115, 331–348.
- Schoene, B., de Wit, M.J., Bowring, S.A., 2008. Mesoarchean assembly and stabilization of the eastern Kaapvaal craton: a structural–thermochronological perspective. *Tectonics* 27, TC5010.
- Sidder, G.B., 1990. Mineral occurrences of the Guiana shield, Venezuela. United States Geological Survey, Open-File Report 90-16 (28 pp.).
- Sidder, G.B., Mendoza, V., 1995. Geology of the Venezuelan Guayana Shield and its relation to the geology of the entire Guayana Shield; U.S. Geological Survey Bulletin 2024, B1–B41.
- Smith, A.G., Livermore, R.A., 1991. Pangea in Permian to Jurassic time. In: Hilde, T.W.C., Carlson, R.L. (Eds.), *Silver Anniversary of Plate Tectonics*. Tectonophysics, 187, pp. 135–179.
- Snowden, P.A., 1984. Non-diapiric batholiths in the north of the Zimbabwe Shield. In: Kröner, A., Greiling, R. (Eds.), *Precambrian Tectonics Illustrated*. Schweizerbart'sche Verlagsbuchhandlung, Stuttgart, pp. 135–145.
- Snowden, P.A., Bickle, M.J., 1976. The Chinamora Batholith: diapiric intrusion or interference fold? *Journal of the Geological Society* 132, 131–137.
- Stockwell, C.H., 1950. The use of plunge in the construction of cross-sections of folds. *Proceedings of the Geological Association of Canada* 3, 97–121.
- St-Onge, M.R., Lucas, S.B., Parrish, R.R., 1992. Terrane accretion in the internal zone of the Ungava orogen, northern Quebec. Part 1: tectonostratigraphic assemblages and their tectonic implications. *Canadian Journal of Earth Science* 29, 746–764.
- Tassinari, C.C.G., Munhá, J.M.U., Teixeira, W., Palácios, T., Nutman, A.P., Sosa, S.C., Santos, A.P., Calado, B.O., 2004. The Imataca Complex, NW Amazonian Craton, Venezuela: Crustal evolution and integration of geochronological and petrological cooling histories. *Episodes* 27, 3–12.
- Van Kranendonk, M.J., Collins, W.J., Hickman, A., Pawley, M.J., 2004. Critical tests of vertical vs. horizontal tectonic models for the Archean East Pilbara Granite–Greenstone Terrane, Pilbara Craton, Western Australia. *Precambrian Research* 131, 173–211.